CONF-861082--1

DEVELOPMENT OF MATHEMATICAL PEDIATRIC PHANTOMS FOR INTERNAL DOSE CALCULATIONS: DESIGNS, LIMITATIONS, AND PROSPECTS*

M. Cristy
Health and Safety Research Division
Oak Ridge National Laboratory
Oak Ridge, Tennessee 37830

MASTER

ABSTRACT

Mathematical phantoms of the human body at various ages are employed with Monte Carlo radiation transport codes for calculation of photon specific absorbed fractions. In the early 1970's, Snyder and co-workers used simple mathematical transformations of their adult phantom to represent children. These "similitude phantoms" represented correctly the differences between adults and children in body shape and relative head-trunk-legs size, but organ sizes and active marrow distributions were not always correct. The author has developed a pediatric phantom series based on the design of the adult phantom, but with explicit equations for each organ so that organ sizes and marrow distributions could be assigned properly. These phantoms are an improvement over those generated by the similitude transformation method. Since the phantoms comprise simple geometric shapes, predictive dose capability is limited when geometry is critical to the calculation, i.e., at low photon energies. Hence, there is a demand for better phantom design in situations where geometry is critical, such as for external irradiation or for internal emitters with low energy photons. Recent advances in computerized axial tomography (CAT) present the potential for derivation of anatomical information, which is so critical to development of phantoms, and ongoing developmental work on computer architecture to handle large arrays for Monte Carlo calculations should make complex-geometry dose calculations economically feasible within this decade.

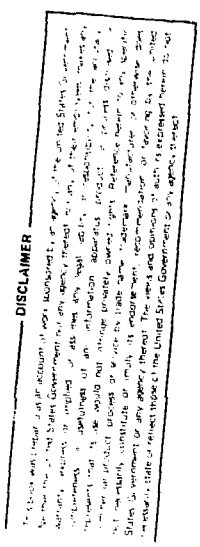

*Research sponsored by the Office of Nuclear Regulatory Research, U.S. Nuclear Regulatory Commission under Interagency Agreement 40-550-75 with the U.S. Department of Energy under contract W-7405-eng-26 with the Union Carbide Corporation.

INTRODUCTION

A series of mathematical phantoms representing children of ages newborn, 1-, 5-, 10-, and 15-years has been developed for use with Monte Carlo photon transport codes. These phantoms, patterned after the Fisher-Snyder adult phantom (1, 2), consist of simple mathematical expressions for the boundaries of the major organs and body sections. As in the adult, three tissue densities are programmed into the transport code -- a low density for lung tissue, a high density for skeletal tissue, and a near unit density for all other tissues. The phantoms are described in detail in Ref. 3.

This report compares earlier phantoms used to represent children in dose calculations, gives selected specific absorbed fraction data based on the present series of phantoms, gives data dealing with geometrical considerations, and discusses prospects in phantom design.

PHANTOM DESIGNS

SIMILITUDES OF THE ADULT PHANTOM

To estimate dose in children, Snyder and co-workers employed so-called "similitude phantoms" (4-9). These phantoms were obtained by transforming the adult phantom. Three orthogonal scaling factors were chosen for each body section (head, trunk, legs) so that the size and shape of each section could be designed to approximate the dimensions of a child of a given age.

The Monte Carlo photon transport code can be used in conjunction with a "similitude phantom" (i.e., a phantom whose major body sections are each a similitude of the corresponding body section in the adult phantom), even though there are no explicit equations for the individual body

INTRODUCTION

A series of mathematical phantoms representing children of ages newborn, 1-, 5-, 10-, and 15-years has been developed for use with Monte Carlo photon transport codes. These phantoms, patterned after the Fisher-Snyder adult phantom (1, 2), consist of simple mathematical expressions for the boundaries of the major organs and body sections. As in the adult, three tissue densities are programmed into the transport code -- a low density for lung tissue, a high density for skeletal tissue, and a near unit density for all other tissues. The phantoms are described in detail in Ref. 3.

This report compares earlier phantoms used to represent children in dose calculations, gives selected specific absorbed fraction data based on the present series of phantoms, given data dealing with geometrical considerations, and discusses prospects in phantom design.

PHANTOM DESIGNS

SIMILITUDES OF THE ADULT PHANTOM

To estimate dose in children, Snyder and co-workers employed so-called "similitude phantoms" (4-9). These phantoms were obtained by transforming the adult phantom. Three orthogonal scaling factors were chosen for each body section (head, trunk, legs) so that the size and shape of each section could be designed to approximate the dimensions of a child of a given age.

The Monte Carlo transport code can be used in conjunction with a "similitude phantom" (i.e., a phantom whose major body sections are each a similitude of the corresponding body section in the adult phantom), even though there are no explicit equations for the individual body

organs but only explicit equations describing the three major body sections. To determine whether a point in a phantom for a given age lies in a particular organ, one uses the adult organ equation and the scaling factors for the appropriate body section. The advantage of this procedure is that one has to provide only the dimensions of the body sections to spawn a phantom with all of the internal organs of the adult phantom. The disadvantage, of course, is that the volumes, shapes, and positions of the internal organs are all determined by the scaling factors and may not be realistic for a particular organ. A review of the treatise on developmental anatomy by Scammon (10) revealed that, for most organs, the shapes and positions are not seriously different from the shapes and positions in a similitude phantom; this can be seen by studying Scammon's Figs. 26-28 and 30-34. In other words, during development, the shapes of the organs often follow body shape, and the relative positions of organs are generally the same. This observation is embodied formally in the Similitude Rule: *For many organs, a similitude transformation of the adult phantom into a child phantom gives a good first approximation to the shapes and the locations of the organs.*

The accuracy of the organ volumes in similitude phantoms is another matter. Cristy and Warner (3) compared similitude organ volumes with mean organ volumes in the newborn child; agreement was fair to good for some organs and poor for others. Another problem with the similitude technique is that the distribution of active bone marrow is not accurately portrayed.

PEDIATRIC PHANTOMS OF HWANG AND CO-WORKERS

Hwang and co-workers developed a series of pediatric phantoms. Descriptions of mathematical phantoms representing ages 0, 1, 5, and 15 years were reported (11-14). Although a phantom representing age 10 was also developed, the description was not published (Hwang, personal communication). These phantoms are similar to the Fisher-Snyder adult phantom in that the basic types of equations for the body sections and organs are the same (e.g., the liver is represented by an elliptical cylinder cut by an oblique plane in all phantoms). These phantoms purport to have organ size, shape, and position determined from anatomical references and thus to be an improvement over the similitude phantoms (11, 15). A careful analysis of the phantom descriptions revealed, however, that for most organs, such as the lungs, the shape in a given pediatric phantom is the same as in the adult phantom, even though the trunk shapes are different in the two cases (by "same shape" is meant, for example, that two ellipsoids have the same shape if one ellipsoid can be transformed into the other by multiplying all three axis lengths by the same factor). Some organs in their descriptions, such as the liver and the ribs, conform to the Similitude Rule.

Having been designed with the same shape as in the adult, the lungs took up a disproportionate length of the trunk in the younger age phantoms. This error resulted apparently from an effort to attain correct lung volumes. Because the lungs were too long and because most adult organ shapes were retained while adult trunk shape was not, severe fitting problems were encountered in the lower trunk. The result was

that organs in the lower trunk had to be shifted around and crowded together, but not in the same manner for each age or in a manner which reflected age-dependent anatomical trends.

PEDIATRIC PHANTOMS OF CRISTY

In designing the adult phantom, Fisher relied heavily upon the excellent cross-section anatomy of adults by Eycleshymer and Schoemaker (16). Too few cross-sectional studies have been done with children to permit the design of pediatric phantoms in the same way. What is known are sizes of organs (17) and general developmental trends, as discussed by Scammon (10). The Similitude Rule was used extensively in designing the pediatric phantoms for ages 0, 1, 5, 10, and 15 years given in this report.

With the Similitude Rule, the design procedure became simple and straightforward: (1) the dimensions of the trunk, the head, and the legs were determined from anthropological data; (2) organ shapes and locations werer determined by the Similitude Rule; (3) organ volumes were determined using masses and specific gravities from ICRP Publication 23 (17); (4) overlapping of organs was eliminated by changing shape, location, or size, depending upon interpretations of drawings and text in *Morris' Human Anatomy* (18) or upon constraints imposed by the simplicity of the phantom design; (5) exceptions to the Similitude Rule were handled individually (e.g., the thymus); and (6) the active marrow distributions were determined.

Average organ volumes rather than masses were used in the design procedure. At present all soft tissue organs of the phantoms are assigned a density ρ of 0.99 g/cm^3 in the photon transport calculations.

Thus, an organ whose density is actually 1.05 g/cm^3 will be represented in a phantom by a space with the correct volume but with a lower mass. In practice this difference is unimportant: the absorbed fraction and the mass are incorrect by approximately the same factor, resulting in a nearly correct specific absorbed fraction. As a practical example, calculations of the specific absorbed fraction of 0.1 MeV photons absorbed in spheres having a uniform distribution of activity were made assuming the that ρ = 1.00 g/cm^3; the data in Table 10 of Ref. 19 were used in these calculations. The error introduced was estimated using the density transformation rule of Loevinger and Berman (20). For spheres ranging in size from 300 to 2000 cm^3 with an actual density of 1.05 g/cm^3, specific absorbed fractions computed as above were in error from -1.8% to +0.6%.

If the design procedure had been to obtain correct masses at the expense of correct volumes, the errors in specific absorbed fractions would have been larger. Using this design procedure in the above example, the errors ranged from -2.9% to -4.4%.

The use of an improved method for estimating the distribution of the active bone marrow for each age (21) is a new feature in these pediatric phantoms. This change is noteworthy because the blood-forming organ is important in the assessment of radiological risk.

With the exception of the newborn, direct information on the distribution of active marrow or total marrow (hematopoietically active marrow plus fatty, inactive marrow) is not known for children. In response to this lack of data, Atkinson (22) derived an approximate method to estimate the distribution of active marrow in children. He

assumed that the distribution of the total marrow spaces in the adult (23) could be used as an approximation to the distribution of total marrow spaces in children. He then applied age-dependent cellularity factors to the marrow space distribution to obtain age-dependent distributions of active marrow (cellularity is defined as the fraction of marrow in a given bone that is active).

The newer method (21) is a modification of Atkinson's method that is simple, yet exhibits numerically large effects at early ages. Factors have been added which take into account that in children the head is proportionately larger and the legs are proportionately smaller than in adults. The method predicts that, in the newborn, 27.8% of the active marrow resides in the skull and 20.7% resides in the lower limbs. By contrast, Atkinson's method predicts 7.0% in the skull and 38.9% in the lower limbs. According to the data of Hudson (24) on the skeletons of 16 late-term fetuses and newborns, 29.5% (±4.2%) of the active marrow resides in the skull, and 23.7% (±2.2%) resides in the lower limbs. The newer method is clearly an improvement.

Snyder (25) pointed out that in considering doses to the active marrow in the newborn and 1-year-old, the doses given for the *total marrow compartment* in the similitude phantoms for these ages could be used, since essentially all of the marrow in infants is active. Note that the similitude technique automatically includes the factors for the relative sizes of the body sections, but does not include cellularity factors. Following the example of Atkinson, Hwang and co-workers failed to include correction factors for relative body section size. Thus, ironically, the procedure suggested by Snyder employing similitude

phantoms would give more meaningful estimates of dose to the active marrow for ages 0-1 year than would be generated employing Hwang's phantom.

Another important change in the phantoms presented here is the addition of female breast tissue, a tissue known to be radiosensitive (26). Female breast tissue appears to be at greatest risk from ionizing radiation during adolescence and early adult life; the breast tissue in female infants and children appears to be at risk also, but the magnitude of this risk is uncertain (27). For prudence' sake, female breast tissue has been included for all ages.

During the development of these pediatric phantoms, several changes were made in the adult phantom. Female breast tissue was added to the trunk, and the improved heart model of Coffey (28) was fitted into the trunk. The lungs had to be redesigned to accommodate the new heart; the difference in size between right and left lungs -- not represented in the Fisher-Snyder phantom -- was incorporated into the new design. The head was redesigned to incorporate the ideas of Hwang, Shoup, and Poston (13), including a change in position of the thyroid. Other minor changes were made so that the adult phantom would be consistent with the manner in which certain organs were fitted into the pediatric phantoms. These latter changes were made not to improve the adult phantom per se but to ensure that age-dependent effects could be assessed.

Figure 1 illustrates the cross-sectional anatomy of the phantoms: superimposed cross-sections of the upper trunk of the adult phantom and the 5- and 1-year-old phantoms are shown. For the adult, cross-sections

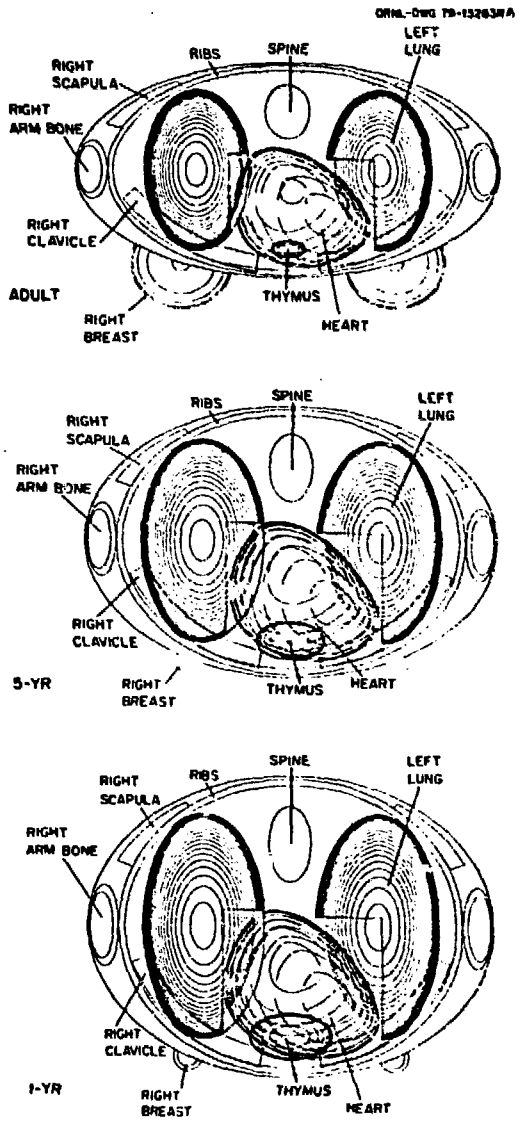

Figure 1. Superimposed cross-sections of the upper trunk of the adult phantom and the 5- and 1-year-old phantoms.

are drawn at intervals of 1 cm. For the other two phantoms, cross-sections are drawn at intervals which yield the same number of sections as for the adult.

SPECIFIC ABSORBED FRACTIONS

Calculations of specific absorbed fractions for various source-target combinations at a range of energies were performed using a Monte Carlo photon transport code. For each source organ, a uniform distribution of activity was assumed and 60,000 photon histories were employed in the calculations. Our computer codes are currently undergoing tests and revisions prior to publication of tables of age-dependent specific absorbed fractions, so these results must be regarded as preliminary.

Table 1 gives an example of a discrete (i.e., not widely distributed) target organ, the ovaries. The specific absorbed fraction increases with decreasing age, with the greatest rate of increase occurring between ages 5-years and newborn. For assessment of the significance of this trend, the ratio of the specific absorbed fraction of a source-to-a-target organ, $\Phi(Y \leftarrow X)$, to the specific absorbed fraction of the source organ-to-itself, $\Phi(X \leftarrow X)$, is given in Table 2. The ratios are expressed in percent.

For discrete targets such as the ovaries, the ratio of the photon dose absorbed by a target organ to the source organ self-dose increases with decreasing age, with the relative increase depending on the energy of the photons and the distance of separation of the source and target organs. These calculations support earlier suggestions (4-9) that cross-organ irradiation is of increased importance in children.

Table 3 gives an example of a distributed target organ, the active marrow, whose distribution changes substantially with age. Here again the specific absorbed fraction increases with decreasing age, since the pathlengths from source to target are smaller for shorter stature. However, when the data are given as the ratio $\Phi(Y \leftarrow X)/\Phi(X \leftarrow X)$, the patterns are more complex (Table 4). For the brain as source organ, the results are similar in pattern to those in Table 2. For the lower large intestine contents, however, the pattern is reversed at the higher three energies, i.e., the ratio is higher in the adult than in children. For the urinary bladder contents the pattern is intermediate, i.e., the ratio changes little with age.

For the photon energies below 0.2 MeV, the values in Tables 3 and 4 are too high by a factor of about 3-4, based on calculations by Eckerman and Simpson (29, 30). This problem arises because the skeleton of the phantom is taken as a homogeneous mixture of bone mineral, marrow, and connective tissue, and the assumption is made that the marrow absorbs energy per gram as efficiently as does the skeletal mixture. This assumption is reasonable at higher photon energies but becomes increasingly inaccurate at energies below 200 KeV. This assumption made by Snyder and colleagues (2) has been a long-standing problem with these calculations (31).

A computational approach to this problem is in sight through the efforts of Keith Eckerman at ORNL. The complex geometry of the tissues in the skeleton still precludes their inclusion in the photon transport calculations. However, the energy deposition in the marrow can be estimated by folding together data on the interactions within the skeletal mixture of a phantom, tabulated during the Monte Carlo photon

transport calculations and the pathlength distributions of trabeculae and marrow spaces of various bones, published by Spiers and colleagues (32). A separate Monte Carlo simulation of secondary electrons liberated within the skeleton, as implemented by Eckerman and Simpson (29), is envisioned to accomplish this task.

GEOMETRY CONSIDERATIONS

The ICRU stated in Report #32 that calculations based on the Fisher-Snyder adult phantom would "generally only provide a very approximate estimate of the absorbed dose received by an actual individual, but they can be valuable to the investigator in indicating whether it is justifiable to carry out a fresh analysis based on a model more closely resembling the dimensions of the individual or group concerned" (33). Calculations based on the series of pediatric phantoms should extend this utility by providing estimates on a wide range of ages and physical sizes.

This section explores a small part of the question, "Just how important is geometry?" For this purpose, calculations were made for the specific absorbed fraction in ellipsoidal targets of various shapes and sizes from a point source (Figs. 2-10) and from sources uniformly distributed in other ellipsoids (Figs. 11-13). These calculations were performed for initial photon energies of 0.05, 0.1, and 1.0 MeV.

An infinite water medium was assumed, and the calculations were simply the integration of the equation for the point isotropic specific absorbed fraction (distance r from a point source),

$$\Phi(r) = \left[\frac{\mu_{en}}{\rho}\frac{e^{-\mu r}}{4\pi r^2}\right]B_{en}(\mu r) \ ,$$

over the volume of the target ellipsoid and over the volume of the source ellipsoid in the case of an extended source. Polynomial equations of degree 9 from Spencer and Simmons (34) were used for the point isotropic energy-absorption buildup factor, $B_{en}(\mu r)$. For the case of a point source, Φ was calculated with a quadrature method at an error tolerance of 0.1%. For the case of extended sources, a random sampling technique (20,000 points in each ellipsoid) was used and the standard deviation of the mean ranged from 2-7%.

In each graph the abscissa is the distance of separation of the center of mass of the target ellipsoid from the point source or the center of mass of the source ellipsoid. At each energy the calculations are made to a maximum distance of separation equal to R_{90}, which is defined as "the radius of a sphere, centered around a point source in water, within which 90% of the source energy is absorbed" (35). Calculations are made to a minimum distance of separation such that the point source is adjacent to the surface of the ellipsoid (Figs. 2-10) or the source and target ellipsoids are just touching (Figs. 11-13).

In each graph the ordinate is the ratio of the specific absorbed fraction in the target ellipsoid calculated as described above to the specific absorbed fraction calculated ignoring spatial geometry, i.e., Φ (center of mass of target ellipsoid ← point source or center of mass of source ellipsoid). Thus the ordinate is a correction factor, the factor by which the simple point-to-point values of Φ would have to be multiplied to correct for the geometry.

A sphere, a thick ellipsoid (principal axes in the ratio of 2/1.5/1), and a flat ellipsoid (principal axes in the ratio 4/2/1) were chosen to test for the effects of shape. These are among the shapes given in MIRD

Pamphlet No. 3 (19) for self-dose calculations. The thick and flat ellipsoids were oriented in each of two ways: with the longest axis directed along the x-axis (designated 2/1.5/1 and 4/2/1 in the figures) or with the shortest axis directed along the x-axis (designated 1/1.5/2 and 1/2/4). The x-axis is defined as the line between the center of mass of the target ellipsoid and the point source or center of mass of the extended source. For clarity of presentation, rectangles of various shapes and orientations are used in the figures to represent the spheres and ellipsoids.

Figure 2 shows the results for target ellipsoids of 1[illegible]d a point source of 0.05 MeV photons. At this energy and for [illegible]get this large, the effects of shape and orientation can be large at [illegible]istances all the way to R_{90}. The curves become quite steep at short distances; but for practical cases of extended sources, this region becomes less important as we will see later in Figs. 11-13.

Figures 3 and 4 show the results for target ellipsoids of 1000 g and point sources of photons of energies 0.1 and 1.0 MeV, respectively, With increasing energy, the effects of shape and orientation are reduced, of course, although they are still too significant to be ignored. In general, both shape and orientation are important in cross-irradiation studies. An orientation of the longest axis of the organ toward the source yields the largest deviation from the point-to-point calculation.

Figures 5-7 show similar results for target ellipsoids of 100 g and point sources of photons of energies 0.05, 0.1, and 1.0 MeV, respectively. For organs of this size, the effects of shape and orientation are much less than in the previous example, especially in the region 0.5 R_{90} to R_{90}.

The effects of organ size are illustrated in Figs. 8-10. Thick target ellipsoids were oriented with the longest axis along the x-axis (2/1.5/1), and the sizes varied from 10 to 1000 g. Energies of photons emitted from a point source were 0.05, 0.1, and 1.0 MeV, respectively. The effect of size is more pronounced in the region from 100 to 1000 g than in the region from 10 to 100 g. At 0.1 and 1.0 MeV, the correction factor is 1.1 or less for most of the sizes illustrated in the distance region 0.5 R_{90} to R_{90}.

Figures 11-13 give the results for the more practical case of an extended source, with uniformly distributed activity and photon energies of 0.05, 0.1, and 1.0 MeV, respectively. For each curve shown, the calculations are based on an ellipsoid pair of sizes 100 and 1000 g. Either ellipsoid may be designated the source, by reciprocity. The ellipsoids are either thick ellipsoids (in various orientations) or spheres. Going from the top to the bottom curve in each figure, the ellipsoid pairs are (orientation in parentheses): 1000 g (2/1.5/1) to 100 g (2/1.5/1); 1000 g (2/1.5/1) to 100 g (1/1.5/2); sphere to sphere; 1000 g (1/1.5/2) to 100 g (2/1.5/1); and 1000 g (1/1.5/2) to 100 g (1/1.5/2). These results are similar to those in Figs. 2-7, except that the sharp rise at the smaller distances is less severe. The results in Figs. 11-13 are approximated by simply adding together (on a logarithmic scale) the appropriate curves in Figs. 2 and 5, 3 and 6, and 4 and 7, respectively, and ignoring the source-target overlap region. Thus the reader may make its own combinations of shapes and orientations and be approximately correct.

In conclusion, geometrical considerations in phantom design are most important for organs larger than about 100 g, for lower energies, and for distances of separation between source and target organs less than about 20 cm. Large differences between the shape and orientation of an organ in the phantom and the shape and orientation of the corresponding human organ can also lead to significant errors.

PROSPECTS IN PHANTOM DESIGN

It is obvious that the utility of calculations employing our simplified geometry phantoms (3) is restricted when the geometry of the individual or group concerned is significantly different from the geometry of any of the phantoms. Of course, the geometry has to be judged with respect to the photon energy and distance of separation, with very sophisticated geometrical detail required for low energy photons. If a dose calculation using our phantoms yields a result close to a dose limit or a radiation protection guideline, the ICRU recommendation (33) of carrying out a fresh analysis should be considered carefully.

Geometry can also be critical in the dosimetry of external irradiation, where the Fisher-Snyder phantom has been used. Recent advances in two areas present the potential for more accurate dose calculations in critical-geometry situations. First, accurate anatomical detail is potentially available through computerized axial tomography (CAT), although (sadly) atlases for different age groups similar in quality to the classic cross-sectional studies of Eycleshymer and Schoemaker (16) have not appeared. Second, advances in computer technology should render Monte Carlo calculations with sophisticated geometries economical

in the years ahead. Monte Carlo techniques are easy to apply, but geometry has been the limiting factor because of costs. Computers have become much faster, and (perhaps of more importance for Monte Carlo calculations) development of computer architecture to handle large arrays is underway (36). With the completion of this developmental work will arise the opportunity to make complex-geometry dose calculations routinely.

Table 1. Specific absorbed fractions, $\Phi(Y \leftarrow X)$, for the ovaries as the target organ.

Energy (MeV)	$\Phi(Y \leftarrow X)$ in kg^{-1}			Target Y ← Source X
	Newborn	5-yr	Adult	
0.015	6.7E-4	0*	0*	Ovaries ← Liver
0.05	6.9E-2	1.3E-2	1.2E-3	
0.2	4.0E-2	9.5E-3	2.2F-3	
1.0	4.2E-2	1.0E-2	2.3E-3	
0.015	1.3E-1	2.8E-3	2.3E-7	Ovaries ← Urinary bladder contents
0.05	3.7E-1	1.2E-1	3.7E-2	
0.2	1.9E-1	6.6E-2	2.4E-2	
1.0	1.9E-1	5.1E-2	2.1E-2	
0.015	4.3E+0	4.8E-1	4.9E-2	Ovaries ← Lower large intestine contents
0.05	8.6E-1	3.0E-1	1.0E-1	
0.2	5.3E-1	1.7E-1	5.9E-2	
1.0	5.0E-1	1.6E-1	4.9E-2	

*No interactions occurred in Monte Carlo code.

Table 2. Ratios of the specific absorbed fraction of a source-to-a-target organ, $\Phi(Y \leftarrow X)$, to the specific absorbed fraction of the source organ-to-itself, $\Phi(X \leftarrow X)$, expressed in percent, for the ovaries as the target organ.

Energy (MeV)	$\Phi(Y \leftarrow X)/\Phi(X \leftarrow X)$ in percent			Target Y ← Source X
	Newborn	5-yr	Adult	
0.015	<0.1	0[a]	0[a]	Ovaries ← Liver
0.05	7.9	4.0	0.8	
0.2	7.5	4.8	2.5	
1.0	7.8	5.6	2.8	
0.015	0.6	<0.1	<0.1	Ovaries ← Urinary bladder contents*
0.05	16	14	8.6	
0.2	13	13	9.5	
1.0	12	9.9	9.1	
0.015	18	9.9	4.3	Ovaries ← Lower large intestine contents*
0.05	40	40	34	
0.2	40	38	34	
1.0	37	37	30	

*For walled organs, $\Phi(X \leftarrow X)$ is defined here as Φ(wall ← contents).

[a]No interactions occurred in Monte Carlo code.

Table 3. Specific absorbed fractions, $\phi(Y \leftarrow X)$, for the active marrow as the target organ.

Energy (MeV)	$\phi(Y \leftarrow X)$ in kg^{-1}			Target Y ← Source X
	Newborn	5-yr	Adult	
0.015	4.4E-1	2.4E-2	5.2E-3	Active marrow ← Brain
0.05	2.6E-1	4.9E-2	1.8E-2	
0.2	5.1E-2	1.2E-2	5.2E-3	
1.0	4.6E-2	1.0E-2	4.2E-3	
0.015	2.0E-1	3.6E-2	4.6E-3	Active marrow ← Lower large intestine contents
0.05	1.8E-1	9.5E-2	4.2E-2	
0.2	3.9E-2	2.3E-2	1.3E-2	
1.0	3.5E-2	1.8E-2	9.0E-3	
0.015	2.2E-3	7.9E-6	0*	Active marrow ← Urinary bladder contents
0.05	9.1E-2	3.9E-2	1.2E-2	
0.2	2.1E-2	1.2E-2	5.7E-3	
1.0	1.8E-2	8.5E-3	3.7E-3	

*No interactions occurred in Monte Carlo code.

Table 4. Ratios of the specific absorbed fraction of a source-to-a-target organ, $\phi(Y \leftarrow X)$, to the specific absorbed fraction of the source organ-to-itself, $\phi(X \leftarrow X)$, expressed in percent, for the active marrow as the target organ.

Energy (MeV)	$\phi(Y \leftarrow X)/\phi(X \leftarrow X)$ in percent			Target Y ← Source X
	Newborn	5-yr	Adult	
0.015	17	3.1	0.8	Active marrow ← Brain
0.05	57	24	9.2	
0.2	18	9.7	4.5	
1.0	16	8.7	3.9	
0.015	0.8	0.7	0.4	Active marrow ← Lower large intestine contents*
0.05	8.7	13	14	
0.2	3.0	5.1	7.3	
1.0	2.6	4.2	5.6	
0.015	<0.1	<0.1	<0.1	Active marrow ← Urinary bladder contents*
0.05	3.8	4.4	2.7	
0.2	1.4	2.3	2.2	
1.0	1.2	1.7	1.6	

*For walled organs, $\phi(X \leftarrow X)$ is defined here as ϕ(wall ← contents).

REFERENCES

1. Fisher, H. L. and Snyder, W. S. Distribution of dose in the body from a source of gamma rays distributed uniformly in an organ. In Proc. First Internat. Congr. Radiat. Protection, Rome, Italy, Sept. 5-10, 1966, pp. 1473-1486. Oxford: Pergamon, 1968.

2. Snyder, W. S., Ford, M. R., Warner, G. G., and Watson, S. B. A tabulation of dose equvalent per microcurie-day for source and target organs of an adult for various radionuclides: Part 1. ORNL-5000, 1974.

3. Cristy, M. Mathematical phantoms representing children of various ages for use in estimates of internal dose. ORNL/NUREG/TM-367, 1980.

4. Snyder, W. S. and Cook, M. J. Preliminary indications of the age variation of the specific absorbed fraction for photons. Health Phys. Div. Annu. Prog. Rep. July 31, 1971. ORNL-4720, pp. 116-118, 1971.

5. Hilyer, M. J. C., Snyder, W. S., and Warner, G. G. Estimates of dose to infants and children from a photon emitter in the lungs. Health Phys. Div. Annu. Prog. Rep. July 31, 1972, ORNL-4811, pp. 91-96, 1972.

6. Snyder, W. S. and Ford, M. R. Estimates of dose rate to gonads of infants and children from a photon emitter in various organs of the body. Health Phys. Div. Annu. Prog. Rep. July 31, 1973. ORNL-4903, pp. 125-129, 1973.

7. Warner, G. G., Poston, J. W., and Snyder, W. S. Absorbed dose in male humanoid phantoms from external sources of photons as a function of age. Health Phys. Div. Annu. Prog. Rep. July 31, 1974. ORNL-4979, pp. 40-45, 1974.

8. Poston, J. W., Snyder, W. S., and Warner, G. G. Age factors for dose rates from an infinite cloud of a photon emitter. Health Phys. Div. Annu. Prog. Rep. June 30, 1975. ORNL-5046, pp. 249-252, 1975.

9. Snyder, W. S., Ford, M. R., Poston, J. W., and Warner, G. G.. Estimates of photon dose to the gonads per microcurie-day as a function of the source organ and the age of the individual. Health Phys. Div. Annu. Prog. Rep. June 30, 1976. ORNL-5171, pp. 27-40, 1976.

10. Scammon, R. E. Developmental anatomy. In Morris' human anatomy, 11th ed., ed. J. P. Schaeffer, pp. 11-62. New York: McGraw-Hill (Blakiston Div.), 1953.

11. Hwang, J. M. L. H., Shoup, R. L., Warner, G. G., and Poston, J. W. Mathematical descriptions of a one- and five-year-old child for use in dosimetry calculations. ORNL/TM-5293, 1976.

12. Hwang, J. M. L., Shoup, R. L., and Poston, J. W. Mathematical description of a newborn human for use in dosimetry calculations. ORNL/TM-5453, 1976.

13. Hwang, J. M. L., Shoup, R. L., and Poston, J. W. Modifications and additions to the pediatric and adult mathematical phantoms. ORNL/TM-5454, 1976.

14. Jones, R. M., Poston, J. W., Hwang, J. L., Jones, T. D., and Warner, G. G. The development and use of a fifteen-year-old equivalent mathematical phantom for internal dose calculations. ORNL/TM-5278, 1976.

15. Poston, J. W. The effects of body and organ size on absorbed dose: there is no standard patient. Radiopharmaceutical Dosimetry Symposium, Oak Ridge, Tenn. HEW Publication (FDA) 76-8044, pp. 92-109, 1976.

16. Eycleshymer, A. C. and Schoemaker, D. M. A cross-section anatomy. New York: Appleton, 1911.

17. International Commission on Radiological Protection. Publication 23. Report of the task group on reference man. Oxford: Pergamon, 1975.

18. Schaeffer, J. P., ed. Morris' human anatomy. 11th ed. New York: McGraw-Hill (Blakiston Div.), 1953.

19. Brownell, G. L., Ellett, W. H., and Reddy, A. R. Absorbed fractions for photon dosimetry. J. Nuc. Med., Suppl. No. 1, MIRD Pamphlet No. 3, pp. 27-39, February, 1968.

20. Loevinger, R. and Berman, M. A revised schema for calculating the absorbed dose from biologically distributed radionuclides. MIRD Pamphlet No. 1, Revised, Society for Nuclear Medicine, New York, 1976.

21. Cristy, M. Active bone marrow distribution as a function of age in humans. (Submitted for publication, Phys. Med. Biol.).

22. Atkinson, H. R. Bone marrow distribution as a factor in estimating radiation to the blood-forming organs. J. Coll. Radiol. Aust. 6: 149-154, 1962.

23. Mechanik, N. Untersuchungen uber das Gewicht des Knochenmarkes des Menschen. Z. Anat. Entwicklungs-Gesch. 79: 58-99, 1926.

24. Hudson, G. Bone-marrow volume in the human foetus and newborn. Brit. J. Haemat. 11: 446-452, 1965.

25. Snyder, W. S. Private communication to J. K. Poggenburg, 1977.

26. International Commission on Radiological Protection. Publication 26. Recommendations of the International Commission on Radiological Protection, Annals of the ICRP, Vol. 1, No. 3. Oxford: Pergamon, 1977.

27. United Nations Scientific Committee on the Effects of Atomic Radiation. Sources and effects of ionizing radiation. General Assembly, Official Records: Thirty-Second Session, Supplement No. 40 (A/32/40), New York, 1977.

28. Coffey, J. L. A revised mathematical model of the heart for use in radiation absorbed dose calculations. M.S. thesis, Univ. Tenn., Knoxville, 1978.

29. Eckerman, K. F. and Simpson, R. Absorbed dose from photoelectrons to the radiosensitive tissue of bone, presented at the 1980 Health Physics Society meeting, July 1980.

30. Eckerman, K. F. Private communication, 1980.

31. Ashton, T. and Spiers, F. W. Attenuation factors for certain tissues when the body is irradiated omnidirectionally. Phys. Med. Biol. 24, 950-963, 1979.

32. Whitwell, J. R. and Spiers, F. W. Calculated beta-ray dose factors for trabecular bone. Phys. Med. Biol., 21, 16-38, 1976.

33. International Commission on Radiation Units and Measurements. Methods of assessment of absorbed dose in clinical use of radionuclides. ICRU Report 32, pp. 36-37, Washington, 1979.

34. Spencer, L. V. and Simmons, G. L. Improved moment method calculations of gamma-ray transport application to point isotropic sources in water. Nuc. Sci. Eng. 50, 20-31, 1973.

35. Reference 33, p. 27.

36. Kalos, M. H. In: A review of the theory and application of Monte Carlo methods. Proceedings of a Seminar-Workshop, Oak Ridge, Tennessee, April 21-23, 1980. (D. K. Trubey and B. L. McGill, eds.). ORNL/RSIC-44, p. 5, 1980.

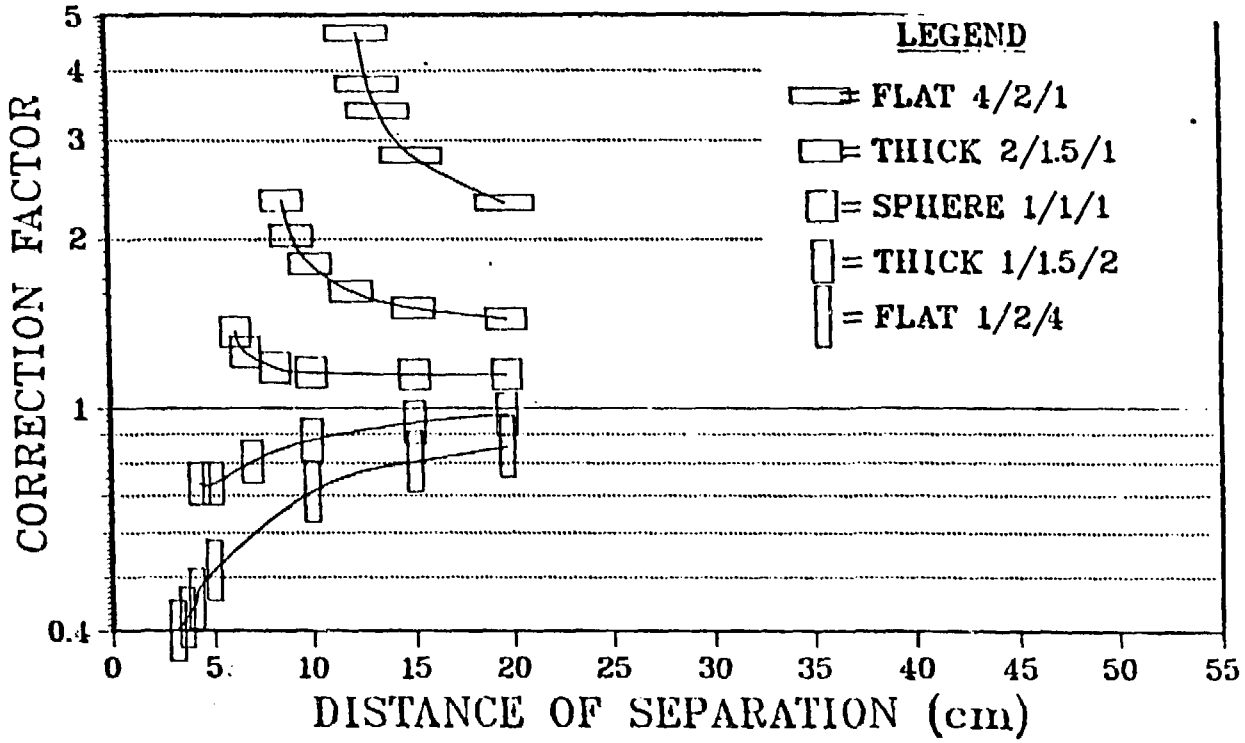

Fig. 2. Geometrical correction factors for 1000 g ellipsoids of various shapes and orientations vs distance of separation from a point source of 0.05 MeV photons, up to a distance of R_{90}.

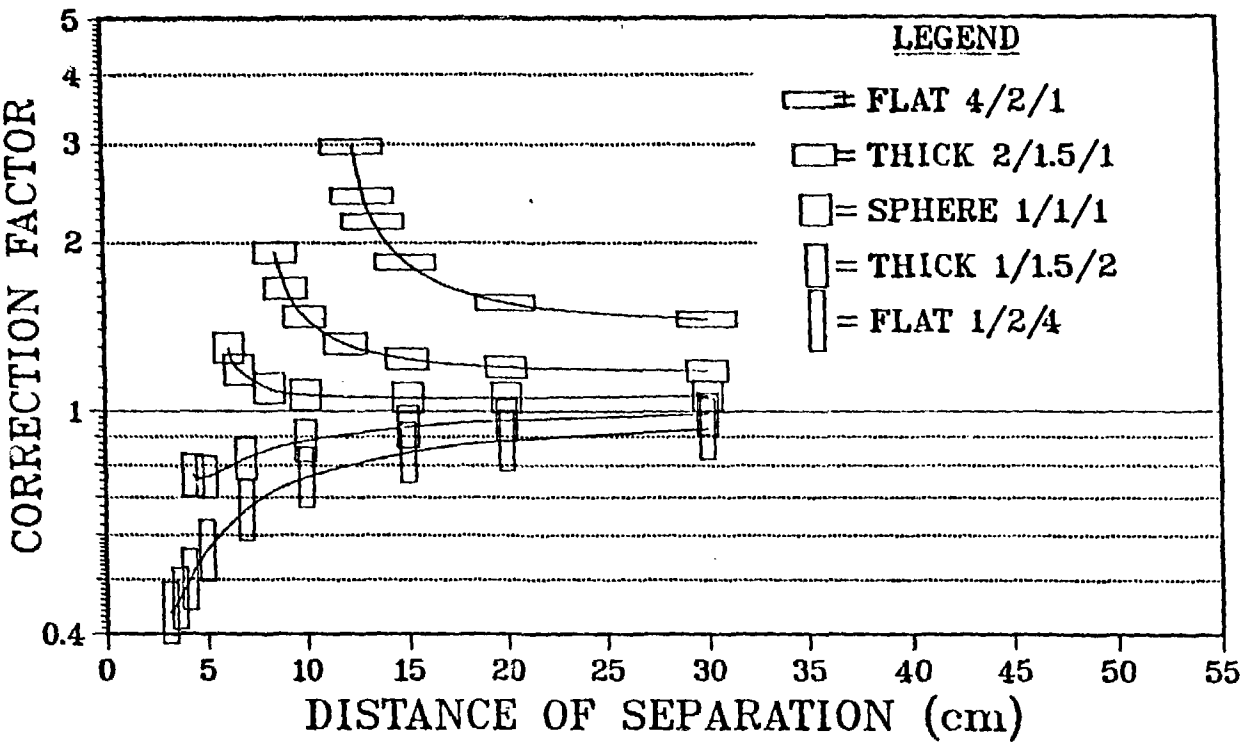

Fig. 3. Geometrical correction factors for 1000 g ellipsoids of various shapes and orientations vs distance of separation from a point source of 0.1 MeV photons, up to a distance of R_{90}.

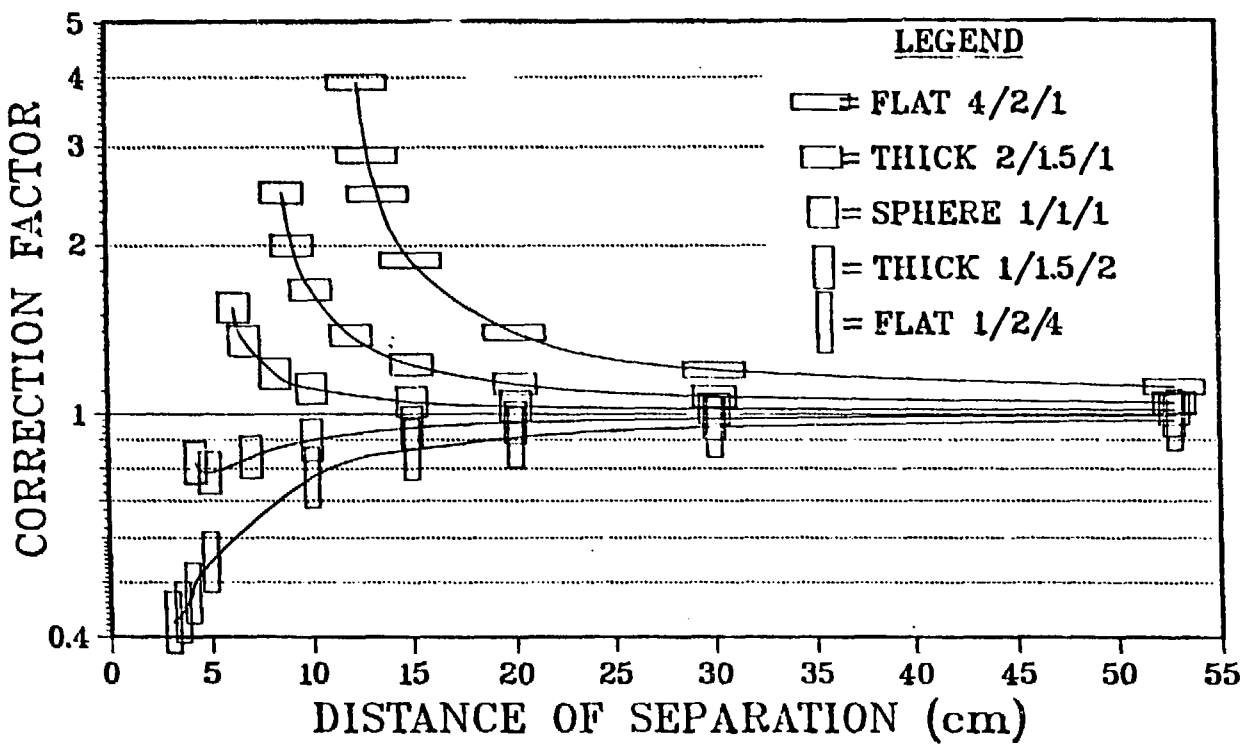

Fig. 4. Geometrical correction factors for 1000 g ellipsoids of various shapes and orientations vs distance of separation from a point source of 1.0 MeV photons, up to a distance of R_{90}.

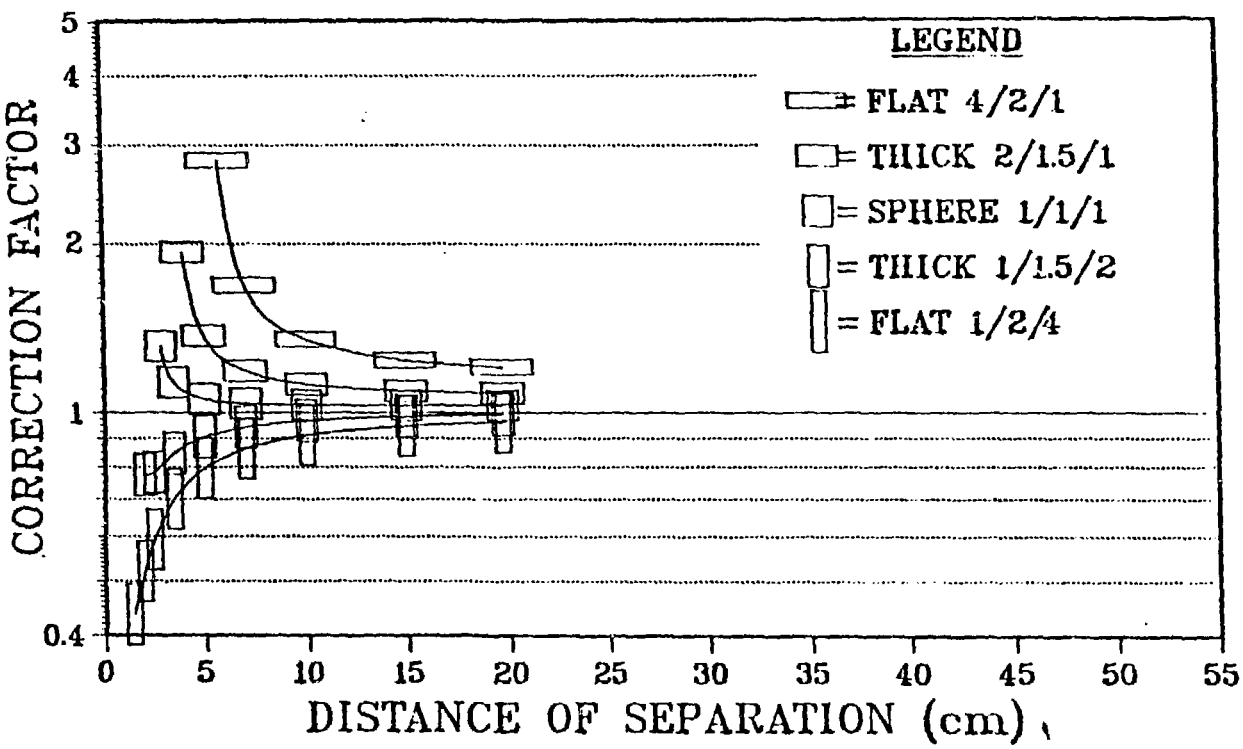

Fig. 5. Geometrical correction factors for 100 g ellipsoids of various shapes and orientations vs distance of separation from a point source of 0.05 MeV photons, up to a distance of R_{90}.

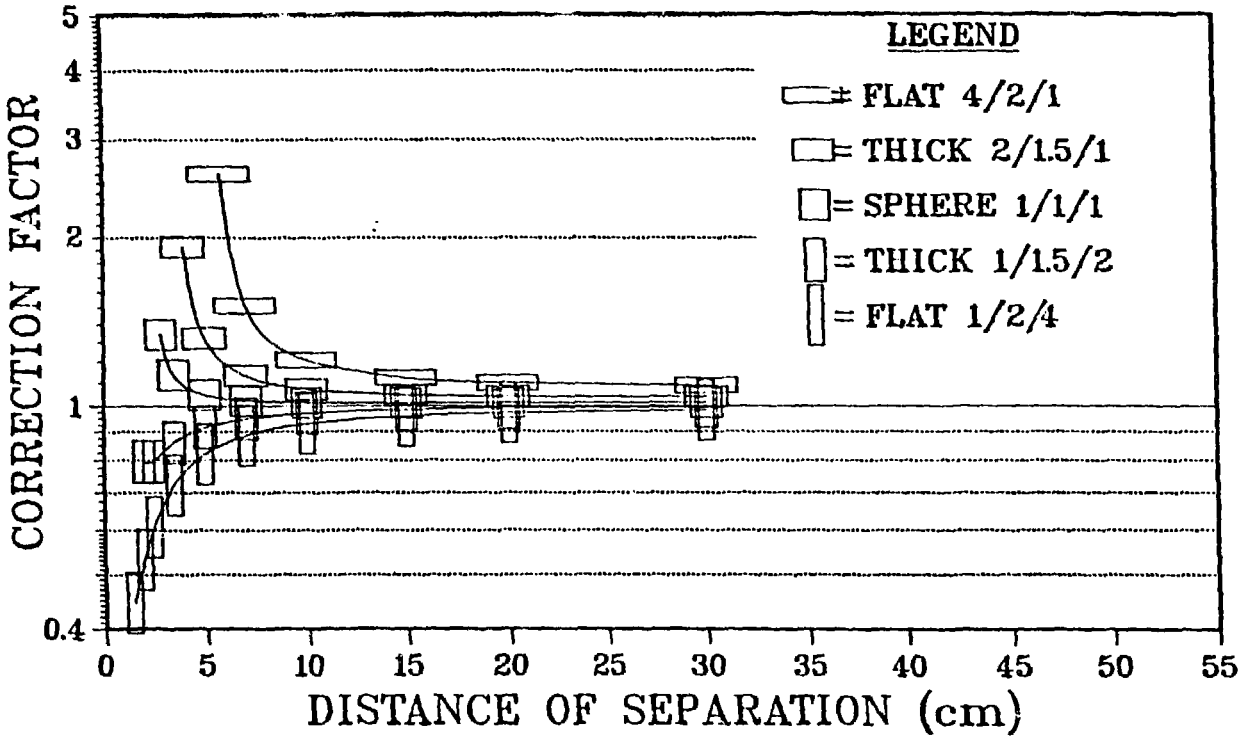

Fig. 6. Geometrical correction factors for 100 g ellipsoids of various shapes and orientations vs distance of separation from a point source of 0.1 MeV photons, up to a distance of R_{90}.

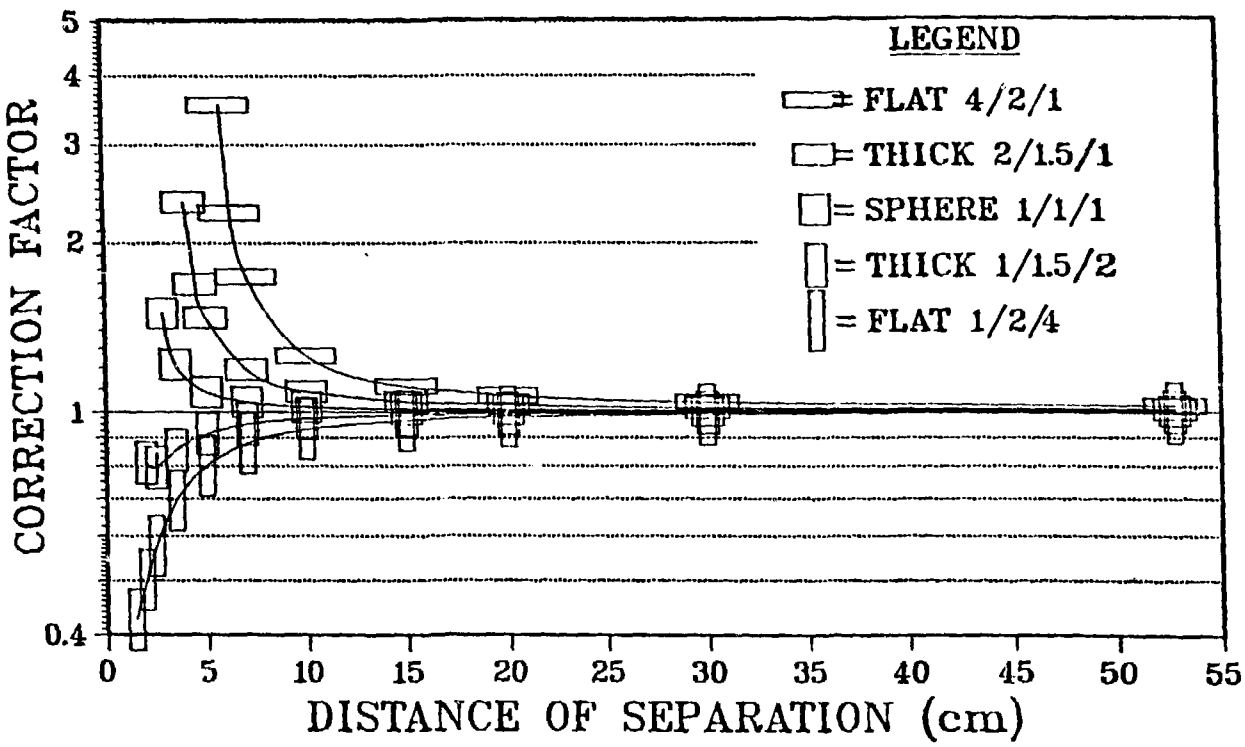

Fig. 7. Geometrical correction factors for 100 g ellipsoids of various shapes and orientations vs distance of separation from a point source of 1.0 MeV photons, up to a distance of R_{90}.

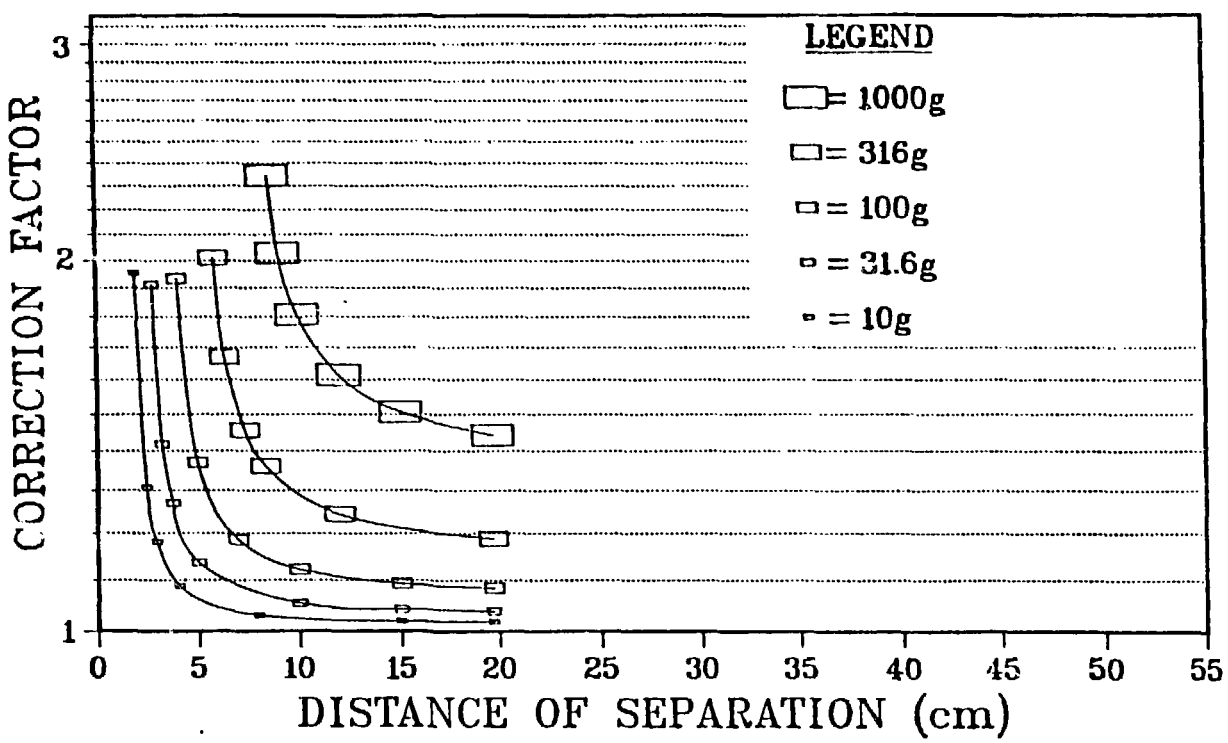

Fig. 8. Geometrical correction factors for thick ellipsoids of various sizes, oriented with the longest axis toward the point source, vs distance of separation from a point source of 0.05 MeV photons, up to a distance of R_{90}.

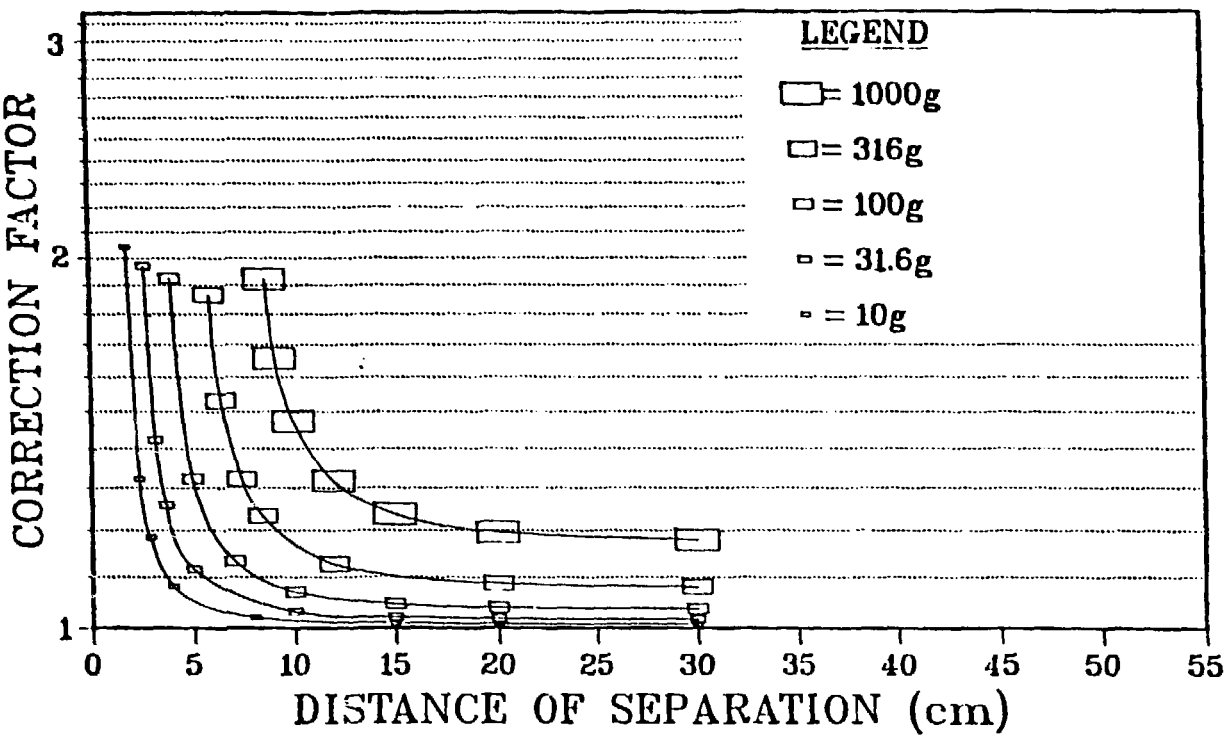

Fig. 9. Geometrical correction factors for thick ellipsoids of various sizes, oriented with the longest axis toward the point source, vs distance of separation from a point source of 0.1 MeV photons, up to a distance of R_{90}.

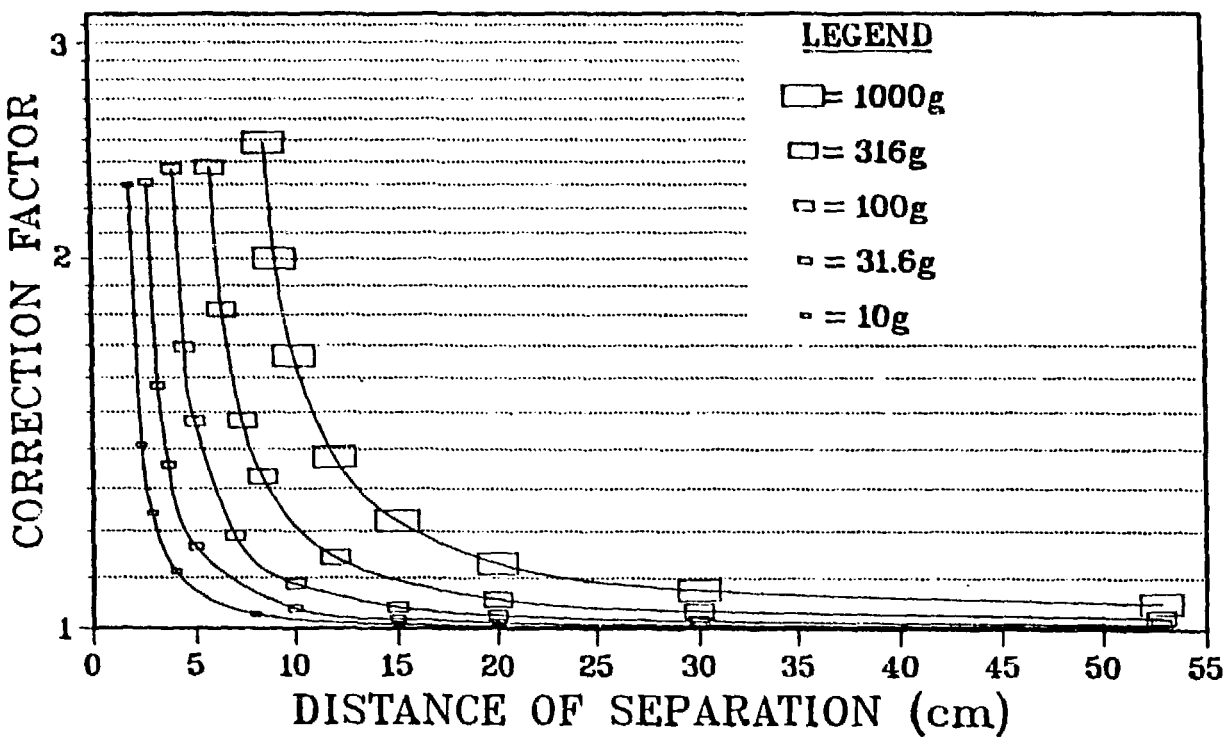

Fig. 10. Geometrical correction factors for thick ellipsoids of various sizes, oriented with the longest axis toward the point source, vs distance of separation from a point source of 1.0 MeV photons, up to a distance of R_{90}.

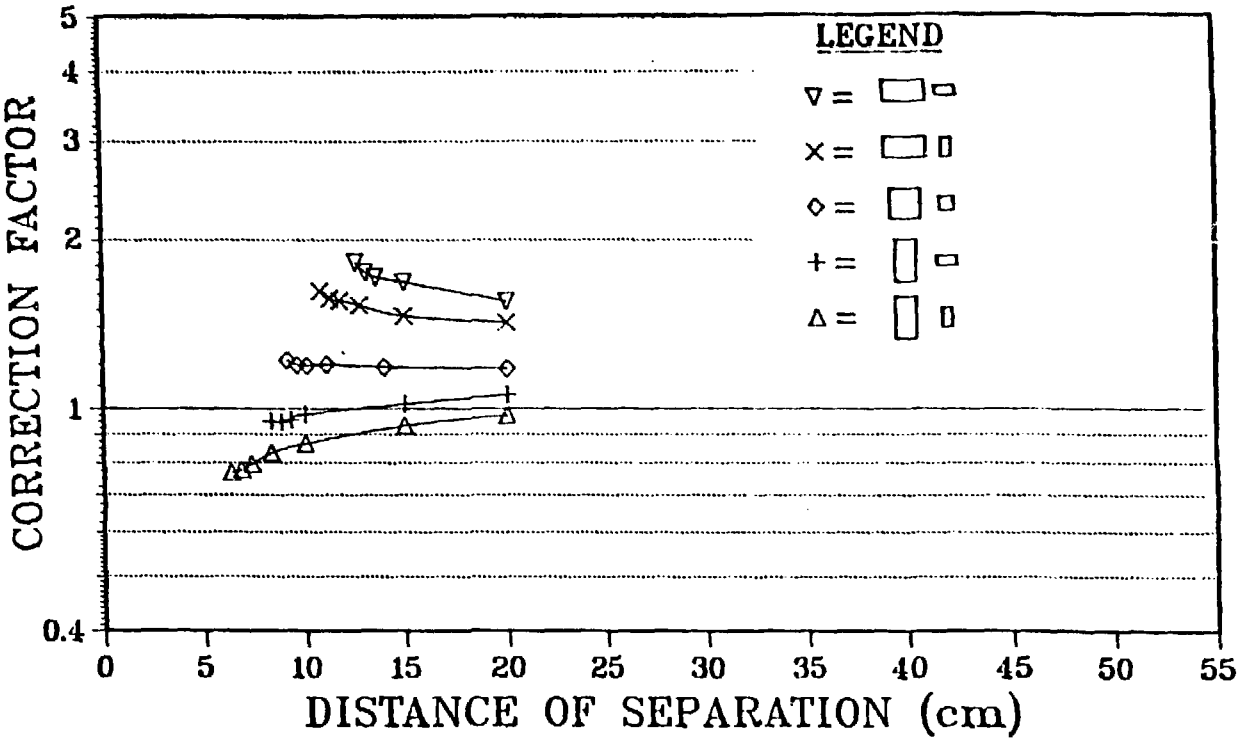

Fig. 11. Geometrical correction factors for selected pairs of ellipsoids vs distance of separation, with one ellipsoid containing a uniformly distributed source of 0.05 MeV photons.

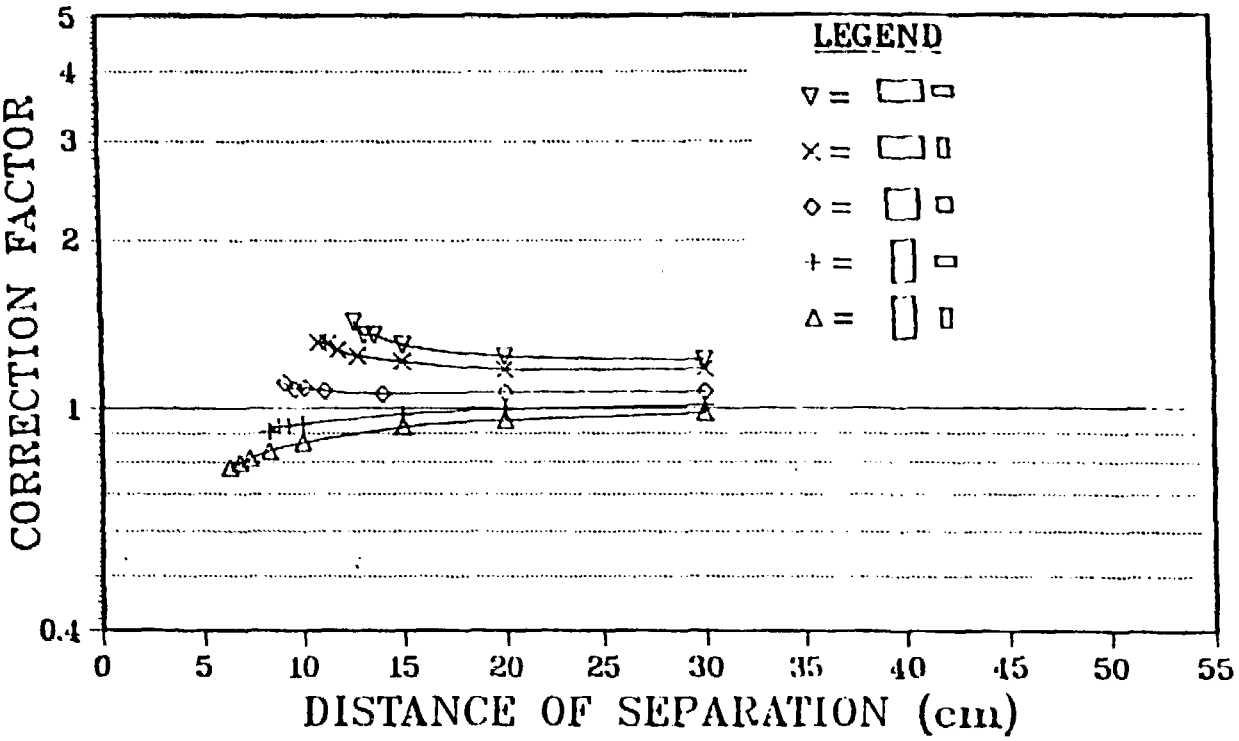

Fig. 12. Geometrical correction factors for selected pairs of ellipsoids vs distance of separation, with one ellipsoid containing a uniformly distributed source of 0.1 MeV photons.

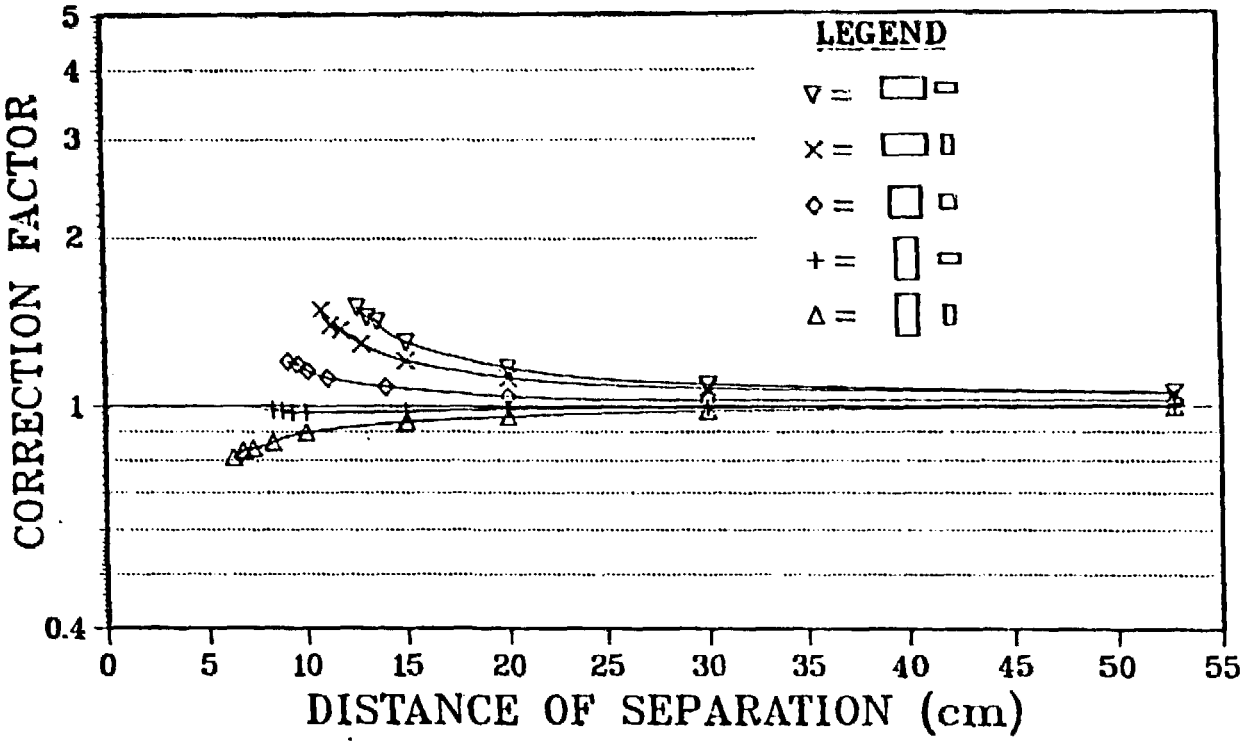

Fig. 13. Geometrical correction factors for selected pairs of ellipsoids vs distance of separation, with one ellipsoid containing a uniformly distributed source of 1.0 MeV photons.